Molecule transfer mechanism in 2D heterostructured lamellar membranes: The effects of dissolution and diffusion

Chongchong Chen[†,※], Xiaoli Wu[†,‡,※], Jie Zhang[†], Jingjing Chen[†], Xulin Cui[†], Wenpeng Li[†], Wenjia Wu[†], Jingtao Wang[†,‡,*]

[†]School of Chemical Engineering, Zhengzhou University, Zhengzhou 450001, P. R. China.
[‡]Henan Institute of Advanced Technology, Zhengzhou University, Zhengzhou 450003, P. R. China.

[※]These authors contributed equally to this work.

E-mail: jingtaowang@zzu.edu.cn (J. Wang).

Abstract

Two-dimensional (2D) lamellar membranes are promising for efficient molecule transfer, while the underlying molecule transfer mechanism is rarely elucidated. Herein, heterostructured nanosheets are prepared by self-assembling small-sized hydrophilic cyanuric acid melamine (CMN) and hydrophobic *g*-C_3N_4 nanosheets. The resultant lamellar membranes show comparable affinity to both polar and nonpolar solvents, allowing them to dissolve on membrane surface and diffuse through membrane channels. Permeance results demonstrate that the transfer of polar solvents is controlled by dissolution and diffusion processes, while that of nonpolar solvents is governed by dissolution process. And the corresponding equations are established. Importantly, polar solvents are induced to form ordered arrangement in hydrophilic nanodomains and then maintain this state in hydrophobic nanodomains, affording low-resistance transfer thus high permeance: 1025 L m^{-2} h^{-1} bar^{-1} for acetonitrile. In contrast, nonpolar solvents with disordered arrangement acquire lower permeance than that of polar ones, but with comparable diffusion ability in these membranes.

KEYWORDS
dissolution and diffusion, molecule transfer mechanism, transfer rate equation, lamellar membrane, hydrophilic/hydrophobic heterostructured nanosheet

1 INTRODUCTION

The newly developed 2D lamellar membranes with well-defined nanostructures display fast molecule transfer and precise sieving, attracting ever-increasing attention in applications of gas capture, water purification and organics recovery, *etc*.[1-4] For instance, the regular channels in MXene lamellar membrane allow molecules transport with low-resistance, and water permeance is over 1000 L m^{-2} h^{-1} bar^{-1}, which is more than 2 orders of magnitude higher than that of state-of-the-art polymer membranes.[5-7] The current attempts are mainly concentrated on manipulating the nanostructures of membrane surface and interlayer channels to enhance molecule permeation.[8-11] However, the underlying molecule transfer mechanism is rarely reported. For example, traditional viewpoint deems that molecule transfer is governed by viscosity that obeys Poiseuille's law.[12-14] While recent works demonstrated that the transfer was also determined by molecule kinetic diameter and solubility parameter, and transfer equations were established based on these parameters.[15] Whereas, dissolution-diffusion mechanism, the typical theory to describe molecule transfer in polymer membranes, has yet been utilized in the investigation for lamellar membranes.

Actually, previous studies have demonstrated that changing the nanostructures of membrane surface and channels, *i.e.*, molecule dissolution and diffusion ability, respectively, alters the transfer rate in lamellar membranes.[16-20] For example, Jiang and co-workers discovered that the permeance of polar and nonpolar solvents were obviously elevated when spraying hydrophilic and hydrophobic polymer clusters on membrane surface, respectively, which enhanced molecule dissolution ability. And the permeance of water and n-hexane were improved from 15.0 and 19.0 L m^{-2} h^{-1} bar^{-1}, to 98.1 and 143.6 L m^{-2} h^{-1} bar^{-1}, respectively.[16] In addition, Thebo *et al*. acquired 2 orders of magnitude higher water permeance than that of primary GO membrane by intercalating theanine amino acid in the channels to manipulate molecule diffusion ability.[18] Differently, Wang and co-workers elevated toluene permeance by less than 1.5 times from 38.5 to 53.3 L m^{-2} h^{-1} bar^{-1} by inserting sodium chloride into GO membrane channels.[20] Analogously, it has demonstrated that polar solvents in hydrophilic

channels form orderly aligned aggregates along channel walls. In contrast, nonpolar solvents are disorderly distributed in hydrophilic channels and diffuse slowly.[21] This indicates that molecule diffusion in channels exerts distinct effect on transport behavior for polar and nonpolar solvents. Albeit these breakthroughs, there is no an explicit cognition about the decisive factor for molecule transfer in lamellar membranes, and the transfer mechanism is still controversial. One basic reason is that the conventional lamellar membranes, which are often assembled by hydrophilic or hydrophobic nanosheets, give obviously distinct affinity to polar and nonpolar solvents.[22,23] The low affinity would repel the dissolution of molecules on membrane surface, thus confounding the effect of diffusion on transfer efficiency. Thus, a platform with comparable affinity is highly desirable for exploring the underlying molecule transfer mechanism.

Hydrophilic/hydrophobic heterostructured nanomaterials, which subtly synergize the superiorities of two materials with reversed hydrophilicity/hydrophobicity, have attracted research interest.[24-27] Heterostructured lamellar membrane with tunable chemical components holds potential for comparable affinity toward both polar and nonpolar solvents, affording equivalent opportunity to dissolve on membrane surface and then have the ability to diffuse in channels. Therefore, heterostructured lamellar membrane should be a desirable platform for exploring molecule transfer mechanism. One recent work designed heterostructured lamellar membrane by adding hydrophobic *g*-C_3N_4 nanosheets into hydrophilic GO interlamination, which boosted water permeance by ten times.[28] Whereas, the interlayer channels are often disordered, and difficult to modulate precisely. In contrast, heterostructured lamellar membrane assembled by hydrophilic/hydrophobic heterostructured nanosheets provides promising platform but are seldom used for studying molecule transfer mechanism.

Herein, heterostructured nanosheets which contain small-sized hydrophilic CMN nanodomains and hydrophobic *g*-C_3N_4 nanodomains were designed as building blocks to assemble heterostructured lamellar membranes. The microstructures and physicochemical

properties of membranes were investigated in detail. Based on this novel platform, molecule transfer mechanism was systematically investigated in terms of water and organic permeance. We demonstrate that the transfer of polar solvents is controlled by dissolution and diffusion processes, while that of nonpolar solvents is governed by dissolution process (Figure 1). And the corresponding equations are established. In addition, heterostructured lamellar membrane achieves obviously enhanced permeance for polar solvents, originating from the excellent dissolution on membrane surface and ultrafast diffusion in channels. The permeance for acetonitrile reaches 1025 L m^{-2} h^{-1} bar^{-1}. While nonpolar solvents acquire relatively lower permeance than that of polar ones but display comparable diffusion in these channels. Furthermore, the well-designed interlayer channels ensure accurate sieving and excellent structural stability for lamellar membranes.

2 MATERIALS AND METHODS

2.1 Materials

Nylon microfiltration substrate with 0.2 μm pore size and 50 mm diameter was purchased from Tianjin Jinteng Experimental equipment Co., Ltd. Melamine and cyanuric acid were supplied from Shanghai Macklin Biochemical Co., Ltd. Concentrated HCl (35% – 37% wt% in water) was obtained by Sinopharm Chemical Reagent Co. Ltd., China. Polydimethylsiloxane (PDMS) was purchased from 3A Chemicals Co., Ltd. Dopamine and *Tris* were supplied by Beijing HWRK Chem Co., Ltd. Organic solvents (acetonitrile, acetone, methanol, isopropanol (IPA), ethyl acetate, ethanol, n-octane n-heptane n-pentane n-hexane, and toluene) were obtained from Tianjin Kemiou Chemistry Reagent Co., Ltd. Acid yellow 14 (AY14), brilliant blue (BB), reactive red (RR), crystal violet (CV), methylene blue (MB) and methyl orange (MO) were supplied from Aladdin Chemical Co., Ltd. These were used as received without further treatment, and deionized water was used throughout the experiment.

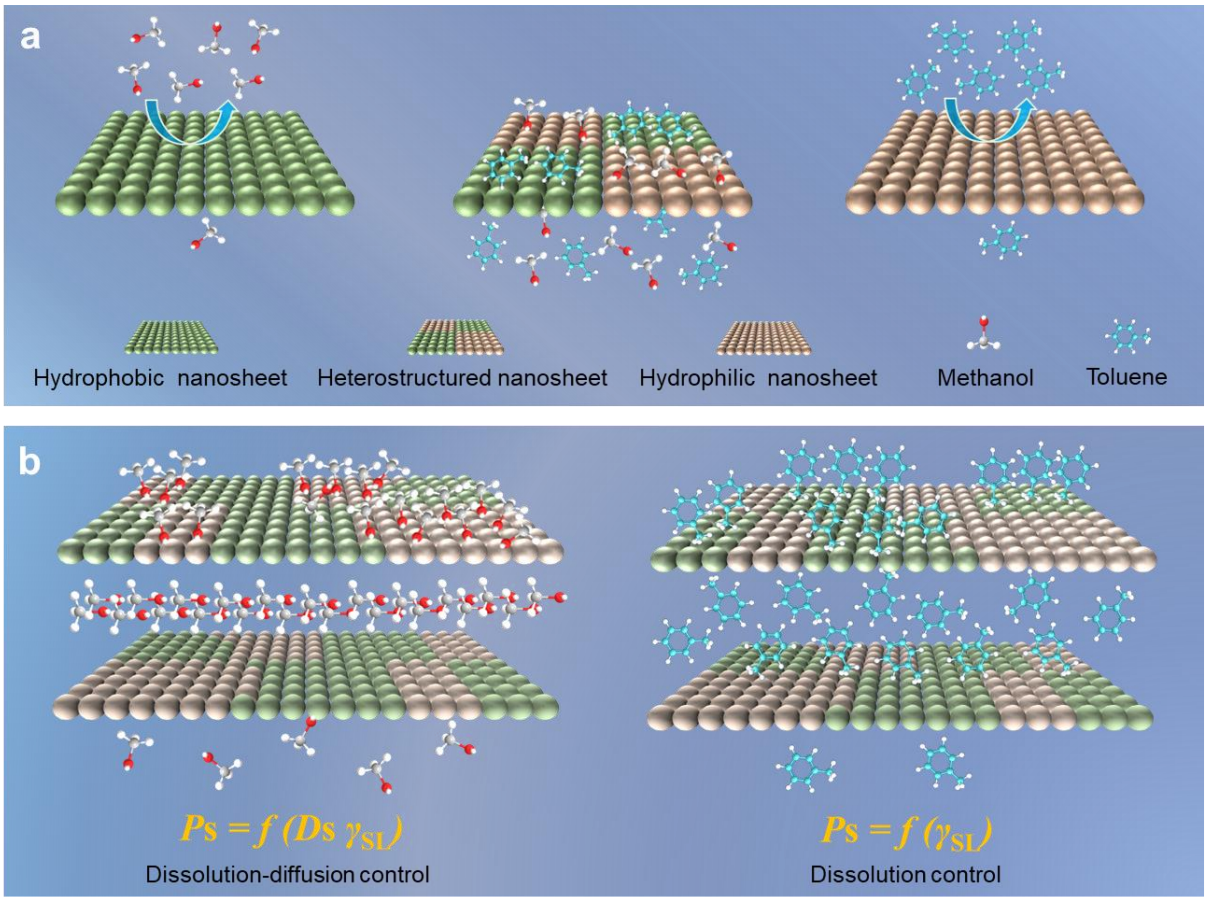

Figure 1. Schematic diagram of (a) dissolution of methanol and toluene on hydrophobic and hydrophilic membrane surfaces, respectively, and (b) the transport in the heterostructured membrane.

2.2 Preparation of heterostructured nanosheets

The small-sized hydrophobic *g*-C_3N_4 nanosheets were obtained by liquid exfoliating of as-prepared *g*-C_3N_4 powder in IPA.[29,30] In detail, 50 mg *g*-C_3N_4 powder was uniformly dispersed in 100 mL IPA. Then, the solution was sonicated for about 16 h and subsequently centrifuged at 6000 rpm to remove residual unexfoliated *g*-C_3N_4 nanoparticles and large-size nanosheets. The lateral size of nanosheets was accurately controlled by tuning the ultrasonic time and centrifugal speed. The small-sized hydrophilic nanosheets were fabricated by classic cyanuric acid and melamine self-assembly.[31] In detail, 2.0 g mixture of cyanuric acid and melamine with a molar ratio of 1:1 was dissolved in 100 mL ethanol to ensure horizontal growth. Then, they were mixed for 1 h using automatic shaker at 30 ℃. The mixture was washed several times with ethanol to remove unpolymerized cyanuric acid and melamine. The resultant powder was vacuum dried at 60 ℃. Then, 50 mg powder was uniformly dispersed in 100 mL

IPA and sonicated for 10 min, and then the dispersion was centrifuged at 6000 rpm to remove large-area nanosheets. Meanwhile, the heterostructured nanosheets were fabricated by a self-assembled strategy. In detail, 50 mL *g*-C_3N_4 nanosheets supernatant solution was uniformly mixed with 50 mL hydrophilic CMN supernatant liquid and stirred for 1 h at 40 ℃. Importantly, the pH of the mixed dispersion was adjusted to 5.0 by HCl solution to improve the accepting ability of carbonyl groups for nucleophile reagent. Then, the reaction mixture was centrifuged at 5000 rpm and then washed with IPA to pH = 7.0, obtaining the light-yellow powder. 10 mg powder was uniformly dispersed in 100 mL IPA and then sonicated for 5 min to obtain dispersion solution of heterostructured nanosheets.

2.3 Preparation of lamellar membranes

The lamellar membranes with well-defined channels were prepared *via* variable speed vacuum filtration (pressure, 0.2 – 1.0 bar) of nanosheets dispersion on the top of Nylon microfiltration support. To improve the affinity between the Nylon support and nanosheets, the support was pre-treated with dopamine aqueous solution (2 mg mL^{-1}) with 10 mM *Tris*-HCl for 4 h to deposit polydopamine (PDA) layer.[32,33] Moreover, to prepare high-quality lamellar membranes, the nanosheets dispersion liquid was diluted. At the end of filtration, the obtained membrane was immediately immersed in organic solvent to maintain a solvated state.[4,13] The PDMS/*g*-C_3N_4 and PDMS/CMN membranes were fabricated by a similar method. First, PDMS solution (0.1 wt%) was obtained by dissolving in the mixture of ethanol and n-hexane (4:3, w/w). Afterward, the PDMS solution (10 mL) was sprayed, respectively, on CMN and *g*-C_3N_4 membrane surfaces.

2.4 Evaluation of nanofiltration performance

Nanofiltration performance was evaluated on home-made device by measuring the permeance of various solvents and rejection of dye molecules respectively. Note that dye molecules with distinct sizes were dissolved in methanol to obtain the desired concentration (10 mg L^{-1}) for rejection measurement, and the concentration was analyzed by NanoDrop UV-

vis spectrophotometer. The solvent permeance (P, L m^{-2} h^{-1} bar^{-1}) was calculated as the following equation:

$$P = \frac{V_P}{(A \cdot t \cdot \Delta P)} \quad (1)$$

where V_p, A, t, and ΔP represent the permeate volume (L), effective membrane area (m^2), testing time (h), and operating pressure (bar), respectively. The rejection (R, %) was obtained by using the following equation:

$$R = (1 - \frac{C_P}{C_f}) \times 100 \quad (2)$$

where C_p and C_f denote the concentration of permeate side solution and feed solution, respectively. All tests were performed at room temperature and the obtained data were averages of three parallel tests.

2.5 Characterization

The morphology and thickness of nanosheets and membranes were characterized by scanning electron microscopy (SEM, Auriga FIB SEM, Zeiss, Germany) and atomic force microscopy (AFM, Bruker Dimension Fast Scan). The lattice of nanosheet was further observed by high-resolution transmission electron microscopy (HRTEM, Tecnai G2 F20, FEI, U.S.). In addition, chemical compositions of nanosheets and membranes were detected by energy-dispersive spectroscopy (EDS) on Auriga FIB SEM, X-ray photoelectron spectroscopy (XPS, AXIS Supra, Kratos, UK) and Fourier transform infrared (FTIR) with the wavelength from 400 – 4000 cm^{-1} (Nicolet MAGNA-IR560 instrument). X-ray diffraction (XRD) was measured on Bruker D8 Advance ECO with the solvated state of membrane samples. N_2 adsorption isotherms were tested for the membranes on automated gas sorption analyzer (Quantachrome Ltd., America). Moreover, the contact angle was tested with FACE (model OCA 25, Germany) at room temperature.

3 RESULTS AND DISCUSSION

3.1 Characterization of heterostructured nanosheet

The heterostructured CM/C_3N_4 nanosheets were prepared by self-assembling small-sized hydrophilic CMN and hydrophobic *g*-C_3N_4 nanosheets in weakly acidic IPA (Figure 2a; Figure S1). During the preparation process, amino groups on the edges of *g*-C_3N_4 nanosheets bonded with hydroxyl/carbonyl groups on the edges of CMN nanosheets through Schiff base reaction and hydrogen-bonding interactions, as proved by FTIR and XPS. Figure S2 shows that compared with primary CMN, the intensity of C=N peak on CM/C_3N_4 enhances obviously, confirming the Schiff base reaction between amino and carbonyl groups. Besides, this peak gives a red shift from 1670 to 1630 cm^{-1}, verifying the formation of hydrogen bonds between nanosheets.[34,35] In addition, the increment of sp^2-bonded N in triazine rings (C–N=C) at 398.7 eV and the decrement of terminal amino groups (–NH_2 / –NH–) at 401.3 eV in XPS spectra also verify the reaction (Figure S3). This mild reaction well maintains the sheet structure of CM/C_3N_4 without visible holes and bulges, as confirmed by SEM and AFM images (Figure 2b; Figure S4). CM/C_3N_4 nanosheets possess typical 2D structure with lateral size of ~ 2 μm and height of ~ 1.1 nm. Considering that the lateral size of CMN and *g*-C_3N_4 nanosheets are ~ 92 and 87 nm, respectively, the CM/C_3N_4 nanosheet is probably bonded by ~ 10 pieces of CMN and *g*-C_3N_4 nanosheets alternately with edge-to-edge structure (Figures S1 and S5).[29-31] This can be directly verified by the HRTEM images in Figure 2d and Figure S6. The strong multiple hydrogen-bonding networks of CMN nanosheets give clear lattice structure, while *g*-C_3N_4 nanosheets display typical triazine unit structure. Moreover, the *d* values of lattice spacing are 0.299 and 0.324 nm, matching well with the spacing of the (002) crystal planes of CMN and *g*-C_3N_4 nanosheets, respectively (Figure S7).[19,31] Furthermore, EDS mappings (Figure 2c; Figure S8) reveal that C and N elements are evenly distributed on nanosheet surface, while O element which only belongs to CMN appears clumped distribution, further confirming the alternate structure of CM/C_3N_4 nanosheet.

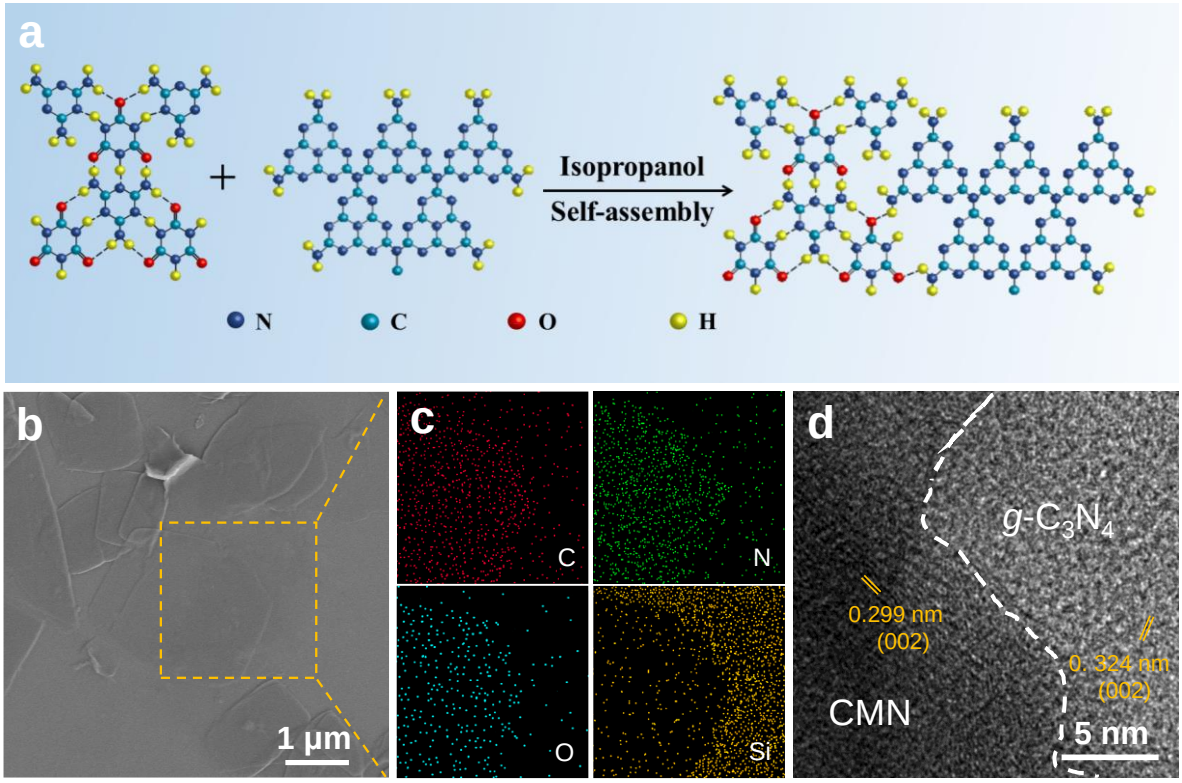

Figure 2. Proofs for the synthesis of CM/C_3N_4 nanosheet. (a) Schematic illustration of the assemble process for CM/C_3N_4 nanosheet. (b) SEM image, (c) corresponding elemental mappings of C, N, O, and Si, and (d) HRTEM image of CM/C_3N_4 nanosheet.

3.2 Morphologies and microstructures of lamellar membranes

Next, the nanosheets were uniformly dispersed in IPA and then slowly stacked on Nylon substrate through vacuum filtration to assemble lamellar membranes (Figure S9). Slow filtration procedure ensures the ordered stacking of nanosheets, forming straight and regular interlayer channels in membrane.[36,37] This is identified by the smooth membrane surface and ordered layer-by-layer stacking of nanosheets in cross-sectional SEM images (Figure 3a and b; Figures S10 – S12). The ordered stacking of nanosheets brings a sharp (002) peak at 2θ = 6.7° in XRD patterns (Figure 3c), corresponding to the close interlayer spacing of ~ 1.3 nm for these lamellar membranes.[38,39] Specifically, hydrophobic *g*-C_3N_4 membrane gives the interlayer spacing of 1.27 nm. While the abundant hydroxy and carbonyl groups on CMN and CM/C_3N_4 nanosheets support a slightly larger interlayer spacings of 1.32 and 1.33 nm, respectively, for lamellar membranes. This can be further verified by the N_2 adsorption-desorption isotherms and pore-size distribution (Figure S13). The *g*-C_3N_4 membrane displays

a pore diameter of 1.17 nm and pore volume of 0.28 cm^{-3} g^{-1}, which are close, but slightly lower than that of CMN (1.23 nm and 0.31 cm^{-3} g^{-1}) and CM/C_3N_4 (1.21 nm and 0.29 cm^{-3} g^{-1}) membranes. Here, membrane thickness is controlled by nanosheet loading (Figure S14), and a thickness of around 1310 nm is selected considering the favorable structural stability.

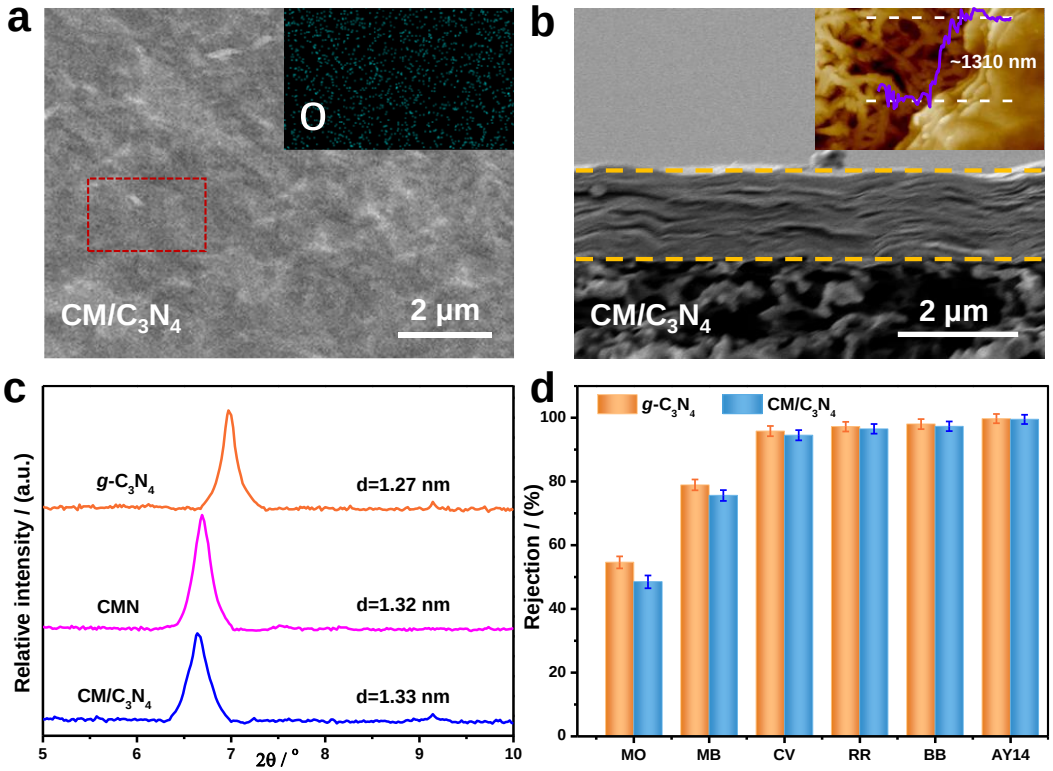

Figure 3. Characterization for the microstructures of lamellar membranes. (a) Surface SEM image of CM/C_3N_4 membrane (inset: elemental mapping of O). (b) Cross-sectional SEM image of CM/C_3N_4 membrane (inset: cross-sectional AFM image and corresponding height profile). (c) XRD patterns of membranes in solvated state. (d) Dye rejection of *g*-C_3N_4 and CM/C_3N_4 membranes.

The highly regular, similar channels of lamellar membranes are further supported by the precise rejection for dyes (Figure 3d). Here, six common industrial dyes with distinct sizes and charges were dispersed in methanol and separated through the membranes (Table S1 and Figure S15). It shows that the rejection of all membranes for methylene blue with size of 1.2 nm is only ~ 75%, while it lifts to over 90% when dye size increases to 1.5 nm (CV). Further increasing dye size to 1.9 nm (acid yellow14) elevates the rejection to nearly 100% (Figures S16 and S17). These imply that the channel size lies between 1.2 and 1.5 nm, and the close rejection results indicate that all membranes possess similar interlayer channels. Note that CM/C_3N_4 membrane with weak negative property gives comparable rejection for negatively

charged reactive red and positively charged CV. This indicates the negligible effect of electrostatic repulsion between dye and membrane on rejection.[40]

3.3 Wettability and solvent uptake of lamellar membranes

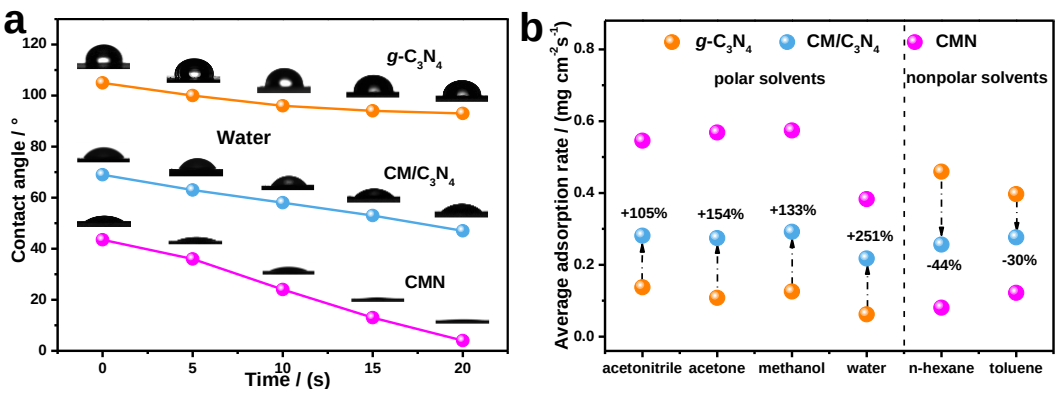

Figure 4. Proofs for the hydrophilicity/hydrophobicity of lamellar membrane. (a) Water contact angles and (b) average adsorption rates of membranes.

These membranes display different wettability as confirmed by the time-dependent water contact angles because of the distinct chemical components. Figure 4a shows that *g*-C_3N_4 membrane gives high water contact angle of over 93° for 20 s, resulting from the hydrophobic character of *g*-C_3N_4 nanosheets.[28] While the water contact angle substantially reduces from 43° to 4° during 20 s for CMN membrane, highlighting the hydrophilic feature of CMN nanosheets. Interestingly, CM/C_3N_4 membrane exhibits moderate reduction of water contact angle from 69° to 47° within 20 s because of the amphipathic property of CM/C_3N_4 nanosheets. Moreover, this further brings distinct dissolution ability for lamellar membranes to polar and nonpolar solvents, as verified by the average adsorption rate of solvents (Figure 4b). Hydrophilic CMN membrane acquires the highest adsorption rate for polar solvents but the lowest value for nonpolar ones. As examples, acetonitrile and acetone acquire the average adsorption rates of 0.54 and 0.57 mg cm^{-2} s^{-1}, respectively, while those of n-hexane and toluene are only 0.08 and 0.12 mg cm^{-2} s^{-1}, respectively. In contrast, hydrophobic *g*-C_3N_4 membrane gives favorable adsorption for nonpolar solvents but poor adsorption for polar ones. Considering that the interlayer space of these membranes is similar, that is comparable storage spacing, the discrepant adsorption rate should originate from the diverse dissolution ability to

molecules. These indicate that hydrophilic CMN membrane has strong dissolution to polar solvents while repels nonpolar ones, and the condition is inverse for hydrophobic *g*-C_3N_4 membrane. Whereas, heterostructured CM/C_3N_4 membrane exhibits comparable affinity and hence dissolution for polar and nonpolar solvents. For instance, the average adsorption rates for acetonitrile and n-hexane are 0.28 and 0.26 mg cm^{-2} s^{-1}, respectively. This further indicates the parallel opportunities to enter into channels for further diffusion.

3.4 Correlation between solvent permeation and dissolution-diffusion

Next, the molecule transfer properties of lamellar membranes were evaluated under pressure of 1 bar by a self-made device after being measured for 3 h to ensure a stable permeance (Figure S18). Note that the Nylon support membrane with large pores (~ 200 nm) exhibits ultrafast molecule permeance (more than 4000 L m^{-2} h^{-1} bar^{-1} for water), but negligible rejection for dyes (Figures S19 and S20).[13] Results show that the lamellar membranes acquire high molecule permeance. The permeances of acetonitrile and acetone reach 1025 and 953 L m^{-2} h^{-1} bar^{-1} for CM/C_3N_4 membrane, respectively, which are more than 2 orders of magnitude higher than that of polymer membranes (Figures 5a and S21). This is attributed to the regular channels that allow continuous and steady molecular-flow with low resistance.[15,41] Here, hydrophobic *g*-C_3N_4 membrane displays excellent permeation for nonpolar solvents as compared to polar ones (Figure S22). For instance, the permeances for n-hexane and toluene are 451 and 354 L m^{-2} h^{-1} bar^{-1}, while those of water and acetone are 188 and 317 L m^{-2} h^{-1} bar^{-1}, respectively. In contrast, hydrophilic CMN membrane gives higher permeance for polar solvents but lower value for nonpolar ones. And the permeances for acetone and n-hexane are 504 and 166 L m^{-2} h^{-1} bar^{-1}, respectively.

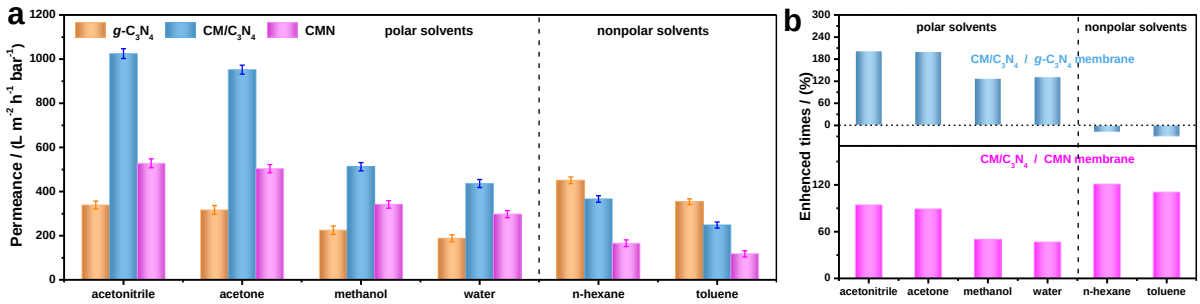

Figure 5. (a) Solvent permeance of the membranes. (b) The upper is the enhanced times of solvent permeance for CM/C_3N_4 to *g*-C_3N_4 membranes and the bottom is that for CM/C_3N_4 to CMN membranes.

Molecules transfer through lamellar membrane should firstly dissolve on membrane surface and then diffuse in inner channels.[1,41,42] The favorable dissolution ability of CMN or *g*-C_3N_4 membranes should be responsible for their high permeation toward polar or nonpolar solvents, respectively. Figure 5b shows that, as compared to hydrophobic *g*-C_3N_4 membrane, introducing hydrophilic nanodomains on CM/C_3N_4 membrane surface permits more than 120% permeance increment for polar solvents. Analogously, the presence of hydrophobic nanodomains on CM/C_3N_4 membrane surface brings substantially elevated permeance for nonpolar solvents as compared to CMN membrane. These findings confirm that the dissolution process governs the transport rate of both polar and nonpolar solvents. For another, it shows that heterostructured CM/C_3N_4 membrane, which possesses comparable solvent dissolution ability, shows much higher permeance for polar solvents than that for nonpolar ones. For example, acetonitrile receives a high permeance of 1025 L m^{-2} h^{-1} bar^{-1}, while that of n-hexane is 366 L m^{-2} h^{-1} bar^{-1}, indicating that diffusion process in inner channels plays distinct role on the transfer of polar and nonpolar solvents. In comparison with CMN membrane, the existence of hydrophobic nanodomains on CM/C_3N_4 membrane, in contrast, gives more than 45% improvement for polar solvents. Considering the depressed dissolution ability of membrane surface, the elevated permeance should result from fast molecule diffusion in inner channels. While nonpolar solvents do not display such specificity. Therefore, polar solvent transfer should be determined by both dissolution and diffusion processes.

3.5 Theoretical analysis of correlations

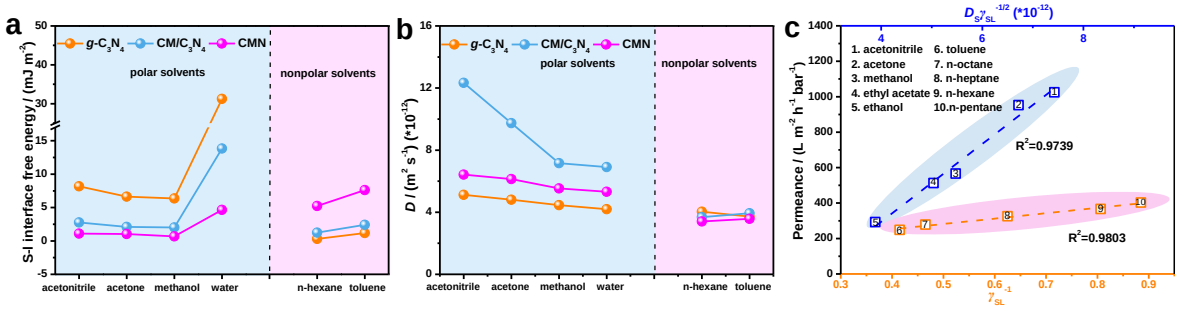

Figure 6. (a) Solid-liquid interface interaction free energy and (b) diffusion coefficient comparison for membranes. (c) The upper is polar solvent permeance against the γ_{SL} and D and the bottom is the nonpolar solvent permeance against for the γ_{SL} for CM/C_3N_4 membrane.

To confirm this hypothesis, the solid-liquid interface interaction free energy (γ_{SL}) and diffusion coefficient (D) are calculated *via* Young's equation (3) and Fick's law (5), respectively (Notes S1 and S2).[21,43]

$$\gamma_S - \gamma_{SL} = \gamma_L \cdot \cos\theta \tag{3}$$

Where γ_S, γ_{SL}, γ_L and θ represent the solid surface energy, liquid surface energy, solid-liquid interface interaction free energy, and contact angle, respectively. The relationship between the γ_S, γ_L, and θ can be expressed as:

$$\cos\theta = -1 + 2 \cdot \sqrt{\frac{\gamma_S}{\gamma_L}} \cdot e^{[-\beta(\gamma_S - \gamma_L)^2]} \tag{4}$$

Where β = 0.000125 (m^2 mJ^{-1})^2.

$$J = -D \cdot \frac{dC}{dx} \tag{5}$$

In equation (5), the D, dC, dx represent the solvent diffusion coefficient (m^2 s^{-1}) in the membrane, concentration difference, diffusion distance (m), respectively. The γ_{SL} results, Figure 6a, corroborate that CMN and CM/C_3N_4 membranes have strong dissolution ability for polar solvents with much lower γ_{SL} values as compared to g-C_3N_4 membrane. While this condition is just inverse for nonpolar solvents, which exhibit well dissolution on g-C_3N_4 and CM/C_3N_4 membranes but barren dissolution on CMN membrane, matching well with the discrepant solvent permeance. This observation demonstrates that the dissolution process on

membrane surface might affect the transfer of both polar and nonpolar solvents. For another, Figure 6b reveals that nonpolar solvents acquire close and low *D* in these lamellar membranes (~ 4.0 × 10^{-12} m^2 s^{-1}). While the *D* values of polar solvents in hydrophilic CMN and amphiphilic CM/C_3N_4 membranes are higher than that in hydrophobic (*g*-C_3N_4) membrane. These phenomena indicate that diffusion process might affect the transfer of polar solvents but exerts negligible effect to that of nonpolar solvents. Note that water molecules possess abnormally high γ_{SL} value for these lamellar membranes. This should be ascribed to the unrivalled surface tension of water, giving weaker dissolution on membrane surface than that of other polar solvents.[44]

Next, the parameters of *D* and γ_{SL} are attempted to quantitatively describe molecule transfer behavior in lamellar membranes. As expected, a transport model that well correlates to the permeance (*P*s) of a polar solvent *s* and the parameters is proposed for CM/C_3N_4 membrane (Figure 6c). The equation can be expressed as:

$$P_s = A \cdot D \cdot \gamma_{SL}^{-1/2} \tag{6}$$

where *A* is a proportionality constant ($mJ^{-1/2}$ m^{-2} bar^{-1}). Note that the equation proposed herein is similar to the one for describing the uncharged organics transport through polymer membranes with uniform free-volume paths:

$$J_s = \frac{\Delta C \cdot (1-\lambda)^2}{\Delta x} \cdot \frac{D_s}{\frac{kT}{\sqrt{e^{\gamma_{SL}}}}} \tag{7}$$

where $\lambda = r_s / r_p$ is the ratio of solute radius (r_s) to the hypothetical membrane pore radius (r_p), *k* and *T* represent the Boltzmann constant (m^2 kg s^{-2} K^{-1}), the absolute temperature (K), respectively. It shows that the polar solvent permeance of the membrane is determined by dissolution and diffusion processes. While the permeances of nonpolar solvents show a relationship as follow:

$$P_s = A' \cdot \gamma_{SL}^{-1} \tag{8}$$

where A' is a proportionality constant (mJ m^{-1} h^{-1} bar^{-1}). The proportional Ps–$\gamma_{SL}^{-1/2}$ relation for polar solvents turns to a Ps–γ_{SL}^{-1} relation for nonpolar ones. This may be ascribed to the weak nonpolar intermolecular interactions, leading to a more significant effect of γ_{SL}.[45,46] This reveals that the nonpolar solvent permeance is mainly governed by dissolution process due to weak channel-molecule interactions. These two equations clearly verify the distinct transfer behaviors of polar and nonpolar solvents, and more importantly, they give new viewpoint in transfer mechanism of lamellar membrane.[47-49] Note that the above equations can only be established by heterostructured membranes, while single hydrophilic or hydrophobic membrane fails to do so. This is mainly because that, the heterostructured membrane allows comparable surface affinity for diverse molecules. This can avoid molecule insolubility on membrane surface, thus confounding the effect of diffusion for transfer.

3.6 The effect of dissolution and diffusion on solvent permeation

Based on the above transfer mechanism, pressure-dependent molecule permeance was measured as shown in Figure 7. The permeance of n-hexane experiences a huge rise from 167 to 386 L m^{-2} h^{-1} bar^{-1} in CMN membrane against the pressure from 1.0 to 5.0 bar, while the permeance maintains at around 445 L m^{-2} h^{-1} bar^{-1} for g-C_3N_4 membrane. This suggests that pressure acts as driving force for nonpolar solvent entering into hydrophilic channels, while hydrophobic membrane can directly dissolve them into inner channels.[16,50] After over dissolution enthalpy, n-hexane obtains similar diffusion property in both hydrophilic and hydrophobic channels, as supported by the comparable permeances when pressure reaches 7.0 bar (Figure 7a). Likely, pressure also helps polar solvents to enter into hydrophobic channels when taking acetone as an example. Differently, acetone permeance in CMN membrane is always higher than that in g-C_3N_4 membrane, even overcoming the dissolution enthalpy. This further verifies the determination of diffusion process on polar solvent transfer (Figure 7b). For a direct comparison, a thin polymer layer of hydrophobic polydimethylsiloxane was sprayed on the surface of CMN and g-C_3N_4 membranes, which were donated as PDMS/CMN

and PDMS/*g*-C_3N_4, respectively (Figures 7c and S23). In this manner, they possess strong and similar dissolution ability toward solvent molecules. Results show that PDMS/CMN and PDMS/*g*-C_3N_4 membranes display comparable permeance for nonpolar solvents, confirming the similar molecule diffusion behavior. As for polar solvents, hydrophilic channels permit higher permeance for PDMS/CMN membrane than that of PDMS/*g*-C_3N_4 membrane because of its high *D* value.

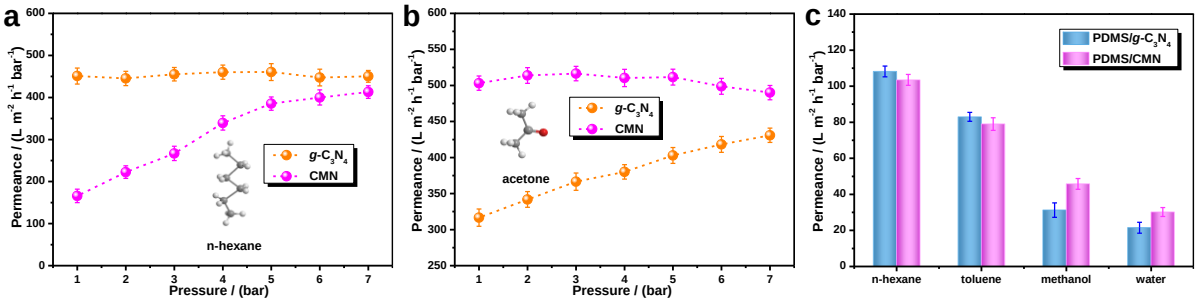

Figure 7. Permeance of (a) n-hexane and (b) acetone as a function of transmembrane pressure for *g*-C_3N_4 and CMN membranes. (c) Solvent permeance of PDMS/*g*-C_3N_4 and PDMS/CMN membranes.

The preliminary results show that heterostructured membrane achieves higher permeance for polar solvents as compared to hydrophilic CMN membrane. For instance, the permeances for acetonitrile and acetone reach 1025 and 953 L m^{-2} h^{-1} bar^{-1}, respectively, which are more than 1.8 times of that of CMN membrane. Considering the depressed dissolution ability of membrane surface, the boosted permeance should be originated from the discrepant diffusion ability. Previous studies have demonstrated that molecular configuration significantly affects the diffusion in interlayer channels.[21,51-54] Presumably, the hydrophilic nanodomains drive polar solvents to form orderly aligned aggregates along channel walls through hydrogen-bonding interactions, which permits fast diffusion (Figure 8a). Then, this aligned aggregate state is maintained when passing into the adjacent hydrophobic nanodomains, and the smooth *g*-C_3N_4 boundary allows a slip by low-friction movement.[19,55] This novel synergistic process contributes to the fast diffusion (*i.e.*, high *D* value) in heterostructured channels.

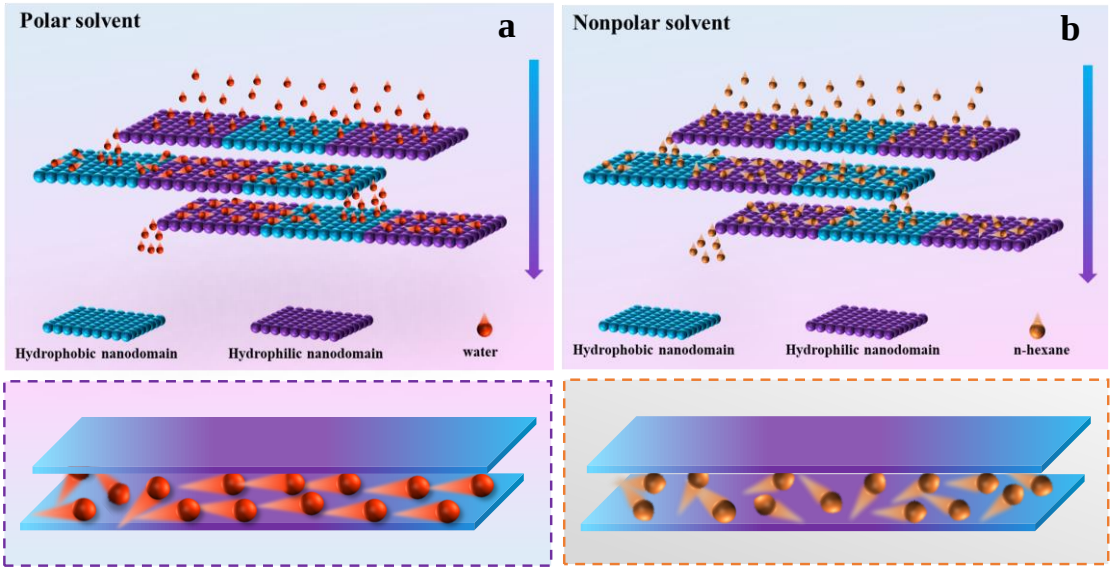

Figure 8. Schematic diagrams of (a) polar solvent molecules and (b) nonpolar solvent molecules transfer from the upper layer to the lower layer in CM/C_3N_4 membrane.

This can be further explored by tuning the respect lateral length of single CMN and *g*-C_3N_4 nanosheets, corresponding to length and ratio of hydrophilic and hydrophobic nanodomains in channels, respectively. Here, the total nanosheet size and membrane thickness are controlled to be comparable. Figure 9a and b reveal that when the lateral lengths of hydrophilic and hydrophobic nanodomains reduced from ~ 90 to ~ 40 nm, it brings conspicuous depression for polar solvent permeance (by ~ 50%) but negligible effect on nonpolar solvent permeance. This should be originated from the fact that hydrophilic nanodomains are too short to fully induce the ordered aggregation of polar solvents. Then, the lateral length of hydrophobic nanodomain was manipulated while maintaining that of hydrophilic nanodomain at ~ 90 nm. We find that acetone permeance drops when ulteriorly boosting the lateral size of hydrophobic nanodomains from ~ 90 to ~ 150 nm (Figure 9c and d). And the corresponding *D* also experiences a reduction from 9.7×10^{-12} to 6.8×10^{-12} m^2 s^{-1}, since the prolonged hydrophobic nanodomain cannot well maintain the ordered molecule aggregation.[53,56] These phenomena highlight the decisive contribution of the synergistic process to fast diffusion in heterostructured channels, matching well with the Arrhenius activation energy of water conduction through membranes (Figure S24).[22,28,57] In contrast, as for nonpolar solvents

(Figure 8b), the weak interactions between channel walls and solvents make them keep disordered distribution state in channels, which would result in random collision among molecules and even collide with channel walls.[15] Thus, a relatively slower transfer occurs resulting from the impaired velocity of molecules as compared with polar solvents.

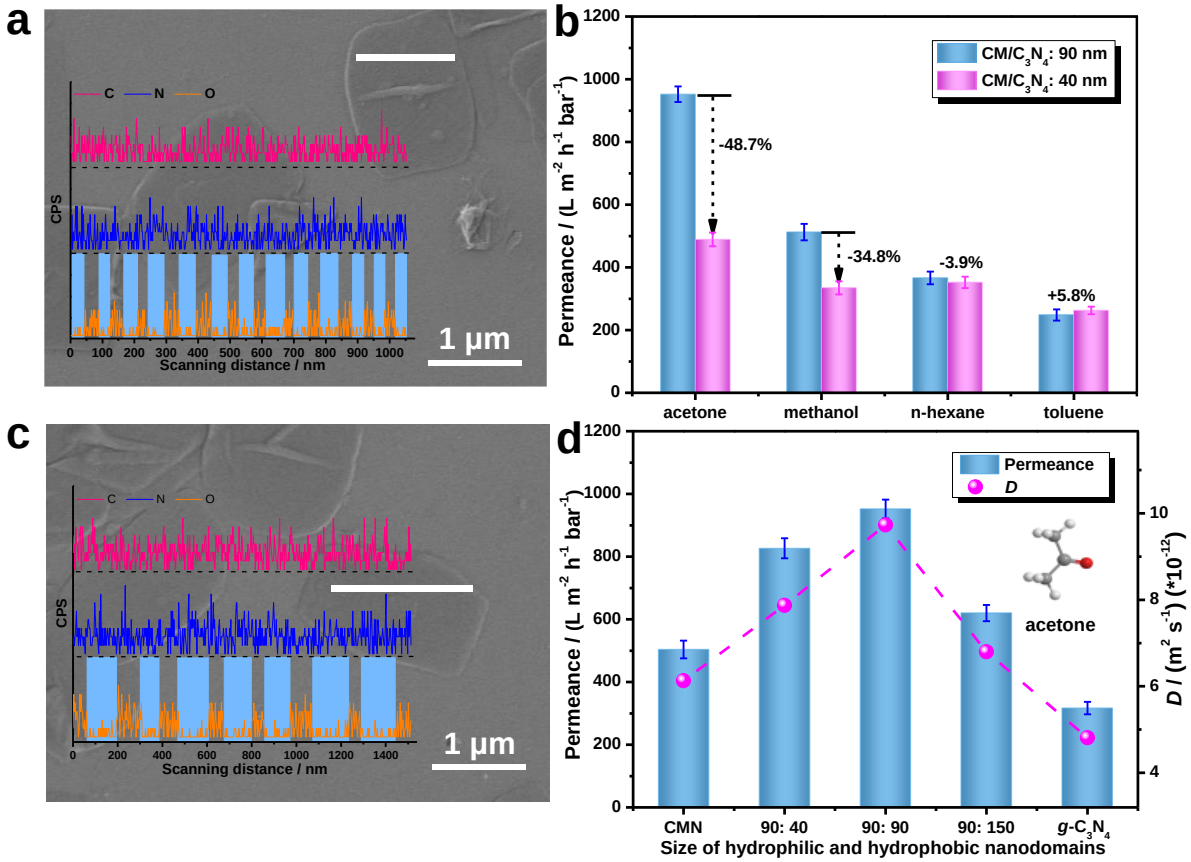

Figure 9. (a) SEM image of CM/C_3N_4 nanosheet with hydrophilic and hydrophobic nanodomain size of about 40 nm (inset: elemental line scanning of C, N, and O). (b) Permeance comparison for CM/C_3N_4 membrane prepared by heterostructured nanosheets with varied size of hydrophilic and hydrophobic nanodomains. (c) SEM image of CM/C_3N_4 nanosheet with hydrophilic and hydrophobic nanodomains of about 90 nm and 150 nm, respectively (inset: elemental line scanning of C, N, and O). (d) Permeance and corresponding *D* comparison for CM/C_3N_4 membrane prepared by heterostructured nanosheets with varied size of hydrophilic and hydrophobic nanodomains.

3.7 Operation stability of lamellar membranes

The structural stability of CM/C_3N_4 membrane was evaluated, which shows that the membrane gives stable performance during a continuous 600 min operation (Figure 10). There is a slight permeance decrease in the initial 2 h, which is ascribed to sheet compaction (Figure 10a). The robust stacking structure also provides favorable pressure resistance for CM/C_3N_4 membrane, which bears the pressure as high as 5.0 bar without structural collapse.

Further increasing the pressure to 6.0 bar brings a variation below 5% in molecule permeance and dye rejection (Figure 10b; Table S2 and Figure S25). Moreover, the intact stacking structure is able to be maintained even soaking in HCl solution for more than 20 min or under ultrasound for 10 min (Figure 10c; Figure S26). Additionally, the amphiphilic and smooth surface of CM/C_3N_4 membrane also acquires outstanding antifouling capability and washing durability (Figure 10d).[16,58]

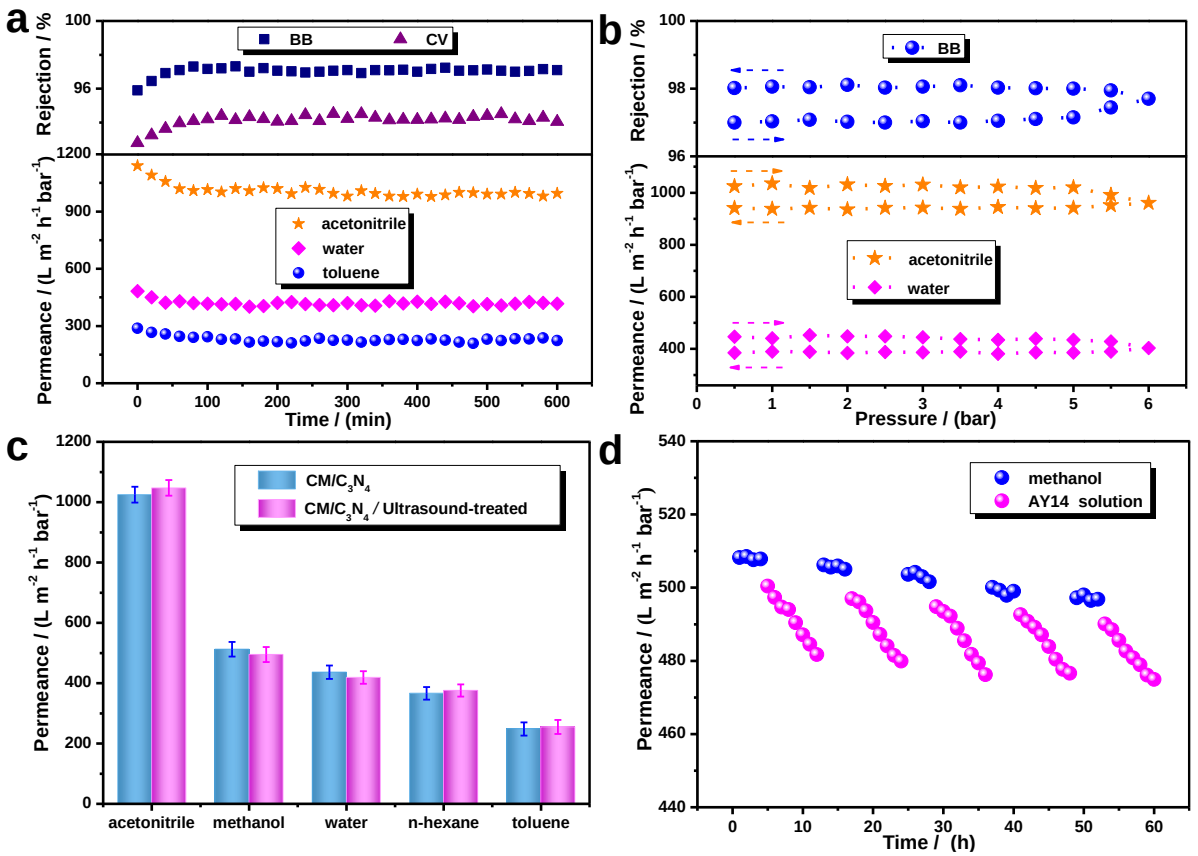

Figure 10. Proofs for the stability of CM/C_3N_4 membrane. (a) Long-term operation performance of CM/C_3N_4 membrane in the permeance of acetonitrile, water, and toluene and rejection of BB and CV under 1 bar. (b) The variation of permeance and rejection of CM/C_3N_4 membrane with transmembrane pressure. (c) Solvent permeance of CM/C_3N_4 membrane before and after ultrasound treatment for 10 min. (d) Demonstration of the low-fouling behavior of CM/C_3N_4 membrane during filtration of an AY14 solution (0.1 g L^{-1}) and permeance recovery after water cleaning in five cycles.

4 CONCLUSIONS

In summary, heterostructured nanosheets assembled by small-sized hydrophilic CMN and hydrophobic *g*-C_3N_4 nanosheets were designed as building blocks to prepare lamellar membranes. Based on this heterostructured platform, we demonstrate that polar and nonpolar solvents show distinct molecule transfer mechanism. The transfer of polar solvents is

controlled by dissolution and diffusion processes, while that of nonpolar solvents is governed by dissolution process. And the corresponding equations are established. Furthermore, we demonstrate that polar solvents are induced to form orderly aligned arrangement along channel walls in hydrophilic nanodomains and then maintain this ordered state in adjacent hydrophilic nanodomains. This permits fast diffusion with low-resistance, giving high polar solvent permeance of 1025 L m^{-2} h^{-1} bar^{-1} for acetonitrile. Moreover, regulating the lateral length and ratio of hydrophilic and hydrophobic nanodomains can manipulate molecule diffusion in heterostructured channels. In contrast, nonpolar solvents with disordered arrangement display comparable diffusion property in all channels, but lower permeance as compared to polar solvents. This elaboration of molecule transfer mechanism in lamellar membranes may provide valuable guidance for rational design of high-efficient separation membranes.

ACKNOWLEDGEMENTS

We gratefully acknowledge the financial support from National Natural Science Foundation of China (No. U1804127), the National Natural Science Foundation of China (No. U2004199), the Natural Science Foundation of Henan Province (212300410285) and the Henan Natural Science Funds for Excellent Young Scholar (202300410373). The Center for advanced analysis and computational science, Zhengzhou University is also gratefully acknowledged.

DATA AVAILABILITY STATEMENT

The data that support the findings of this study are available from the corresponding author upon reasonable request.

AUTHOR CONTRIBUTIONS

Chongchong Chen: Data curation; investigation; writing-original draft; writing-review & editing. **Xiaoli Wu:** Data curation; investigation; software; writing-original draft; writing-review & editing. **Jie Zhang:** Data curation; investigation. **Jingjing Chen:** Software; writing-original draft. **Xulin Cui:** Software; investigation. **Wenpeng Li:** Writing-original draft;

supervision. **Wenjia Wu:** Project administration; supervision. **Jingtao Wang:** Funding acquisition; project administration; supervision; writing-original draft; writing-review & editing.

REFERENCES

1. Liu G, Jin W, Xu N. Two-dimensional-material membranes: a new family of high-performance separation membranes. *Angew Chem Int Ed*. 2016;55:13384−13397.
2. Ding L, Wei Y, Li L, Zhang T, Wang H, Xue J, Ding L, Wang S, Caro J, Gogotsi Y. MXene molecular sieving membranes for highly efficient gas separation. *Nat Commun*. 2018;9:155.
3. Zhou KG, Vasu KS, Cherian CT, Neek-Amal M, Zhang JC, Ghorbanfekr-Kalashami H, Huang K, Marshall OP, Kravets VG, Abraham J, Su Y, Grigorenko AN, Pratt A, Geim AK, Peeters FM, Novoselov KS, Nair RR. Electrically controlled water permeation through graphene oxide membranes. *Nature*. 2018;559:236−240.
4. Huang L, Chen J, Gao T, Zhang M, Li Y, Dai L, Qu L, Shi G. Reduced graphene oxide membranes for ultrafast organic solvent nanofiltration. *Adv Mater*. 2016;28:8669−8674.
5. Ding L, Wei Y, Wang Y, Chen H, Caro J, Wang H. A two-dimensional lamellar membrane: MXene nanosheet stacks. *Angew Chem Int Ed*. 2017;129:1−6.
6. Culp TE, Khara B, Brickey KP, Geitner M, Zimudzi TJ, Wilbur JD, Jons SD, Roy A, Paul M, Ganapathysubramanian B, Zydney AL, Kumar M, Gomez ED. Nanoscale control of internal inhomogeneity enhances water transport in desalination membranes. *Science*. 2021;371:72−75.
7. Echaide-Górriz C, Malankowska M, Téllez C, Coronas J. Nanofiltration thin-film composite membrane on either the internal or the external surface of a polysulfone hollow fiber. *AIChE J*. 2020;66:e16970.

8. Huang K, Liu G, Shen J, Chu Z, Zhou H, Gu X, Jin W, Xu N. High-efficiency water-transport channels using the synergistic effect of a hydrophilic polymer and graphene oxide laminates. *Adv Funct Mater*. 2015;25:5809−5815.

9. Wang Y, Liu L, Xue J, Hou J, Ding L, Wang H. Enhanced water flux through graphitic carbon nitride nanosheets membrane by incorporating polyacrylic acid. *AIChE J*. 2018;64:2181−2188.

10. Zhang WH, Yin MJ, Zhao Q, Jin CG, Wang N, Ji S, Ritt CL, Elimelech M, An QF. Graphene oxide membranes with stable porous structure for ultrafast water transport. *Nat Nanotechnol*. 2021;16:337−343.

11. Lee CS, Choi M, Hwang YY, Kim H, Kim MK, Lee YJ. Facilitated water transport through graphene oxide membranes functionalized with aquaporin-mimicking peptides. *Adv Mater*. 2018;30:1705944.

12. Karan S, Samitsu S, Peng X, Kurashima K, Ichinose I. Ultrafast viscous permeation of organic solvents through diamond-like carbon nanosheets. *Science*. 2012;335:444−447.

13. Yang Q, Su Y, Chi C, Cherian CT, Huang K, Kravets VG, Wang FC, Zhang JC, Pratt A, Grigorenko AN, Guinea F, Geim AK, Nair RR. Ultrathin graphene-based membrane with precise molecular sieving and ultrafast solvent permeation. *Nat Mater*. 2017;16:1198−1202.

14. Huang H, Song Z, Wei N, Shi L, Mao Y, Ying Y, Sun L, Xu Z, Peng X. Ultrafast viscous water flow through nanostrand-channelled graphene oxide membranes. *Nat Commun*. 2013;4:2979.

15. Wang J, Chen P, Shi B, Guo W, Jaroniec M, Qiao SZ. A regularly channeled lamellar membrane for unparalleled water and organics permeation. *Angew Chem Int Ed*. 2018;57:6814−6818.

16. Wang J, Yuan Z, Wu X, Li Y, Chen J, Jiang Z. Beetle-inspired assembly of heterostructured lamellar membranes with polymer cluster-patterned surface for enhanced molecular permeation. *Adv Funct Mater*. 2019;29:1900819.

17. Liang F, Liu Q, Zhao J, Guan K, Mao Y, Liu G, Gu X, Jin W. Ultrafast water-selective permeation through graphene oxide membrane with water transport promoters. *AIChE J*. 2020;66:e16812.

18. Thebo KH, Qian X, Zhang Q, Chen L, Cheng HM, Ren W. Highly stable graphene-oxide-based membranes with superior permeability. *Nat Commun*. 2018;9:1486.

19. Ran J, Pan T, Wu Y, Chu C, Cui P, Zhang P, Ai X, Fu CF, Yang Z, Xu T. Endowing *g*-C_3N_4 membranes with superior permeability and stability by using acid spacers. *Angew Chem Int Ed*. 2019;58:1−8.

20. Long Y, Wang K, Xiang G, Song K, Zhou G, Wang X. Molecule channels directed by cation-decorated graphene oxide nanosheets and their application as membrane reactors. *Adv Mater*. 2017;29:1606093.

21. Wu X, Cui X, Wu W, Wang J, Li Y, Jiang Z. Elucidating the ultrafast molecular permeation through well-defined 2D nanochannels of lamellar membranes. *Angew Chem Int Ed*. 2019;58:18524−18529.

22. Chen C, Wang J, Liu D, Yang C, Liu Y, Ruoff RS, Lei W. Functionalized boron nitride membranes with ultrafast solvent transport performance for molecular separation. *Nat Commun*. 2018;9:1902.

23. Wang Y, Gao B, Yue Q, Wang Z. Graphitic carbon nitride (*g*-C_3N_4)-based membranes for advanced separation. *J Mater Chem A*. 2020;8:19133.

24. Song Y, Li X, Fan JB, Kang H, Zhang X, Chen C, Liang X, Wang S. Interfacially polymerized particles with heterostructured nanopores for glycopeptide separation. *Adv Mater*. 2018;30:1803299.

25. Fu ZJ, Wang ZY, Liu ML, Cai J, Yuan PA, Wang Q, Xing W, Sun SP. Dual-layer membrane with hierarchical hydrophobicity and transport channels for nonpolar organic solvent nanofiltration. *AIChE J*. 2020;67:e17138.

26. Meng X, Wang M, Heng L, Jiang L. Underwater mechanically robust oil-repellent materials: combining conflicting properties using a heterostructure. *Adv Mater*. 2018;30:1706634.

27. Liu J, Hua D, Zhang Y, Japip S, Chung TS. Precise molecular sieving architectures with Janus pathways for both polar and nonpolar molecules. *Adv Mater*. 2018;30:1705933.

28. Wu Y, Fu CF, Huang Q, Zhang P, Cui P, Ran J, Yang J, Xu T. 2D heterostructured nanofluidic channels for enhanced desalination performance of graphene oxide membranes. *ACS Nano*. 2021;15:7586−7595.

29. Zhang X, Xie X, Wang H, Zhang J, Pan B, Xi Y. Enhanced photoresponsive ultrathin graphitic-phase C_3N_4 nanosheets for bioimaging. *J Am Chem Soc*. 2013;135:18−21.

30. Yang S, Gong Y, Zhang J, Zhan L, Ma L, Fang Z, Vajtai R, Wang X, Ajayan PM. Exfoliated graphitic carbon nitride nanosheets as efficient catalysts for hydrogen evolution under visible light. *Adv Mater*. 2013;25:2452−2456.

31. Shalom M, Inal S, Fettkenhauer C, Neher D, Antonietti M. Improving carbon nitride photocatalysis by supramolecular preorganization of monomers. *J Am Chem Soc*. 2013;135:7118−7121.

32. Hu M, Mi B. Enabling graphene oxide nanosheets as water separation membranes. *Environ Sci Technol*. 2013;47:3715−3723.

33. Han Y, Xu Z, Gao C. Ultrathin graphene nanofiltration membrane for water purification. *Adv Funct Mater*. 2013;23:3693−3700.

34. Zhang M, Mao Y, Liu G, Liu G, Fan Y, Jin W. Molecular bridges stabilize graphene oxide membranes in water. *Angew Chem Int Ed*. 2020;59:1689−1695.

35. Shinde DB, Sheng G, Li X, Ostwal M, Emwas AH, Huang KW, Lai Z. Crystalline 2D covalent organic framework membranes for high-flux organic solvent nanofiltration. *J Am Chem Soc*. 2018;140:14342−14349.

36. Xu WL, Fang C, Zhou F, Song Z, Liu Q, Qiao R, Yu M. Self-assembly: a facile way of forming ultrathin, high-performance graphene oxide membranes for water purification. *Nano Lett*. 2017;17:2928−2933.

37. Li W, Wu W, Li, Z. Controlling interlayer spacing of graphene oxide membranes by external pressure regulation. *ACS Nano*. 2018;12:9309−9317.

38. Nie L, Goh K, Wang Y, Lee J, Huang Y, Karahan HE, Zhou K, Guiver MD, Bae TH. Realizing small-flake graphene oxide membranes for ultrafast size-dependent organic solvent nanofiltration. *Sci Adv*. 2020;6:eaaz9184.

39. Wang Y, Wu N, Wang Y, Ma H, Zhang J, Xu L, Albolkany MK, Liu B. Graphite phase carbon nitride based membrane for selective permeation. *Nat Commun*. 2019;10:2500.

40. Wang Z, Tu Q, Zheng S, Urban JJ, Li S, Mi B. Understanding the aqueous stability and filtration capability of MoS_2 membranes. *Nano Lett*. 2017;17:7289−7298.

41. Shen J, Liu G, Huang K, Chu Z, Jin W, Xu N. Subnanometer two-dimensional graphene oxide channels for ultrafast gas sieving. *ACS Nano*. 2016;10:3398−3409.

42. Koltonow AR, Huang J. Two-dimensional nanofluidics. *Science*. 2016; 351:1395−1396.

43. Li D, Neumann AW. Equation of state for interfacial tensions of solid-liquid systems. *Adv Colloid Interface Sci*. 1992;39:299−345.

44. Xiao J, Wen H, Wang L, Xu L, Hao Z, Shao CL, Wang CY. Catalyst-free dehydrative SN1-type reaction of indolyl alcohols with diverse nucleophiles “on Water”. *Green Chem*. 2016;18:1032−1037.

45. Ahmad A, Li SH, Zhao ZP. Insight of organic molecule dissolution and diffusion in cross-linked polydimethylsiloxane using molecular simulation. *J Membr Sci*. 2021;620:118863.

46. Darvishmanesh S, Degreve J, Bruggen BVD. Mechanisms of solute rejection in solvent resistant nanofiltration: the effect of solvent on solute rejection. *Phys. Chem. Chem. Phys*. 2010;12:13333−13342.

47. Huang K, Liu G, Lou Y, Dong Z, Shen J, Jin W. A graphene oxide membrane with highly selective molecular separation of aqueous organic solution. *Angew Chem Int Ed*. 2014;53:6929−6932.

48. Shen J, Liu G, Ji Y, Liu Q, Cheng L, Guan K, Zhang M, Liu G, Xiong J, Yang J, Jin W. 2D MXene nanofilms with tunable gas transport channels. *Adv Funct Mater*. 2018;28:1801511.

49. Ma L, Gutierrez L, Vanoppen M, Lorenz DN, Aubry C, Verliefde A. Transport of uncharged organics in ion-exchange membranes: experimental validation of the solution-diffusion mode. *J Membr Sci*. 2018;564:773−781.

50. Holt JK. Fast mass transport through sub-2-nanometer carbon nanotubes. *Science*. 2006;312:1034−1037.

51. Nair RR, Wu HA, Jayaram PN, Grigorieva IV, Geim AK. Unimpeded permeation of water through helium-leak-tight graphene-based membranes. *Science*. 2012;335:442−444.

52. Gong X, Li J, Lu H, Wan R, Li J, Hu J, Fang H. A charge-driven molecular water pump. *Nat Nanotechnol*. 2007;2:709−712.

53. Hummer G, Rasaiah JC, Noworyta JP. Water conduction through the hydrophobic channel of a carbon nanotube. *Nature*. 2001;414:188−190.

54. Dou H, Jiang B, Xu M, Zhang Z, Wen G, Peng F, Yu A, Bai Z, Sun Y, Zhang L, Jiang Z, Chen Z. Boron nitride membranes with a distinct nanoconfinement effect for efficient ethylene/ethane separation. *Angew Chem Int Ed*. 2019;58:13969−13975.

55. Wang Y, Li L, Wei Y, Xue J, Chen H, Ding L, Caro J, Wang H. Water transport with ultralow friction through partially exfoliated *g*-C_3N_4 nanosheet membranes with self-supporting spacers. *Angew Chem Int Ed*. 2017;56:1−7.

56. Li J, Gong X, Lu H, Li D, Fang H, Zhou R. Electrostatic gating of a nanometer water channel. *Proc Natl Acad Sci USA*. 2007;104:3687−3692.

57. Liu J, Wang, N.; Yu, L.-J.; Karton, A.; Li, W.; Zhang, W.; Guo, F.; Hou, L.; Cheng, Q.; Jiang, L.; Weitz, D. A.; Zhao, Y. Bioinspired graphene membrane with temperature tunable channels for water gating and molecular separation. *Nat. Commun*. 2017,8,2011.

58. Zhang R, Li Y, Su Y, Zhao X, Liu Y, Fan X, Ma T, Jiang Z. Engineering amphiphilic nanofiltration membrane surfaces with a multi-defense mechanism for improved antifouling performances. *J Mater Chem A*. 2016;4:7892−7902.